Open access • Journal Article • DOI:10.1088/1361-6595/AB3CFC

Electric field evolution in a diffuse ionization wave nanosecond pulse discharge in atmospheric pressure air — Source link

Tat Loon Chng, Alexandra Brisset, Pascal Jeanney, Svetlana Starikovskaia ...+2 more authors

Institutions: École Polytechnique, Université Paris-Saclay, Ohio State University

Published on: 24 Sep 2019 - Plasma Sources Science and Technology (IOP Publishing)

Topics: Voltage, Electric field, Ionization, Field (physics) and Plasma

Electric field evolution in a diffuse ionization wave nanosecond pulse discharge in atmospheric pressure air

Tat Loon Chng, Alexandra Brisset, Pascal Jeanney, Svetlana Starikovskaia, Igor Adamovich, Pierre Tardiveau

Electric Field Evolution
in a Diffuse Ionization Wave Nanosecond Pulse Discharge in Atmospheric Pressure Air

T. L. Chng[1], A. Brisset[2], P. Jeanney[2], S. M. Starikovskaia[1], I.V. Adamovich[3] and P. Tardiveau[2]

[1] *Laboratory of Plasma Physics (CNRS, Ecole Polytechnique, Sorbonne Universities, University Paris-Sud), Institut Polytechnique de Paris, route de Saclay, 91128 Palaiseau,* France

[2] *LPGP, CNRS, Univ. Paris-Sud, Université Paris-Saclay, 91405, Orsay, France*

[3]*Nonequilibrium Thermodynamics Laboratories, Department of Mechanical and Aerospace Engineering, Ohio State University, Columbus, OH 43210, USA*

Abstract

The time-resolved electric field in a fast ionization wave discharge in a diffuse nanosecond pulse discharge plasma in atmospheric pressure air is measured using the Electric Field Induced Second Harmonic (E-FISH) diagnostic. The electric field is placed on an absolute scale by calibration against a Laplacian field. At relatively low peak voltages, when the plasma is generated only near the pin high-voltage electrode, the electric field is measured ahead of the ionization wave during the entire voltage pulse, exhibiting a strong field enhancement compared to the Laplacian field, by about an order of magnitude. As the peak voltage is increased and the ionization wave traverses the laser beam, the electric field is measured both ahead of the wave and behind the ionization front, where the field drops rapidly due to the charge separation and plasma self-shielding. When the wave reaches the grounded electrode, the discharge transitions into a conduction phase in which the potential is redistributed within the gap. The electric field in the vicinity of the pin then increases again, following the applied voltage waveform for the rest of the pulse. The effective time resolution of the present measurements is 150 ps. Based on the single shot data, we find that the peak electric field in the wave front is moderately influenced by the applied voltage and varies between 160 to 210 kV/cm. This study demonstrates the viability of the E-FISH diagnostic for this class of atmospheric pressure discharges and paves the way for future in-depth studies of this particular problem.

1. Introduction

Generation and quantitative characterization of reproducible, volumetric ionization wave discharges in atmospheric pressure gas mixtures present a significant challenge. As discussed in [1,2], diffuse ionization waves are generated at high overvoltages (defined as the ratio of the pulse peak voltage to the DC breakdown threshold [3]), when the rate of electron impact ionization exceeds that of the charge separation and plasma self-shielding. This requires the use of pulse waveforms with a high voltage rise rate (on the order of ~10 kV/ns in room temperature, atmospheric pressure air), and short pulse durations (on the order of ~10 ns), to prevent transition to a spark discharge in the conduction phase [2,4]. At these conditions, pulsed breakdown develops as a single large-scale ionization wave, rather than a well-defined streamer or an ensemble of streamers [2,4]. The formation of a single ionization wave may also be affected by non-local kinetics of high-energy electrons and photons produced in the wave front, generating pre-ionization ahead of the wave [1,2]. Transition between the different modes of the ns pulse discharge development, such as corona, glow, and spark [5-7], as well as the diffuse-to-filamentary mode transition [2,4], have been primarily studied using plasma emission imaging and optical emission spectroscopy, as well as numerical modeling [8-12].

Kinetics of ionization, charge transport, and energy partition in these discharges are of significant interest both from a fundamental viewpoint, and for engineering applications such as plasma-assisted combustion [13] and development of soft X-ray sources [14,15]. One of the greatest difficulties in the quantitative analysis of these discharges is a lack of non-intrusive measurements of the transient electric field, as well as electron density and temperature, with sufficiently high spatio-temporal resolution. In a recent study [16], the electric field in a pin-to-plane ns pulse discharge in atmospheric pressure air (peak voltage 68 kV, rise time 3 ns, discharge gap 15 mm) was measured using an electro-optic probe [17], with a time resolution of ~ 1 ns and spatial resolution of ~ 1 mm (peak electric field up to 70 kV/cm, ionization wave speed ≈ 1 cm/ns). However, based on numerical modeling predictions [4], the characteristic spatial and time scales of the electric field variation in the ionization wave generated in air at similar conditions (peak voltage 50 kV, rise time rate 2 ns, discharge gap 10 mm), are ~ 300 μm and ~ 50 ps, respectively, at a peak electric field of 100 kV/cm and wave speed of 0.25 cm/ns. In addition, inserting the probe into the plasma may well result in perturbations due to surface charge accumulation on the probe housing. Therefore, fully resolving the ionization wave front, and potentially detecting the non-local electron kinetics effects, requires the use of non-intrusive, ultra-short pulse (fs to ps) laser diagnostics. Development of such diagnostics is critical for gaining quantitative insight into the kinetics of ionization waves in high-pressure plasmas sustained by ns pulse discharges.

The objective of the present work is to measure the electric field in the fast ionization wave of a ns pulse discharge in atmospheric pressure air in the pin-to-plane geometry, at conditions similar to those of [4,16]. In the present experiments, we use the ps Electric Field Induced Second Harmonic (E-FISH) diagnostic developed in [18,19], which is capable of sub-ns time resolution, limited by the laser pulse duration, the detector rise time, and the sampling rate of the oscilloscope. Recently, ps four-wave mixing, as well as ps and fs E-FISH measurements, have been made in atmospheric pressure ns pulse discharges in ambient air and argon [20-22], and in a ns pulse discharge in 100 Torr of air [23]. In [23], a relatively weak ionization wave propagating between the discharge electrodes has been identified. In the present work, the wave front is expected to be more pronounced, due to the much higher pressure and the small radius of curvature of the high-voltage electrode.

2. Experimental and Data Reduction

The experimental apparatus, shown in Fig. 1, is the same as the one used in [4]. Briefly, a diffuse ns pulse discharge is sustained in a pin-to-plane geometry across a 16 mm gap, with the pin high-voltage electrode on top, as shown schematically in Fig. 1. The pin electrode, made of tungsten, has a parabolic shape, with a tip curvature radius of 50 μm. The plane grounded electrode is a copper plate 50 mm in diameter. The pin electrode is powered by a ns pulse voltage waveform produced by an FID FPG 50-1NMX3A15 high-voltage pulse generator, with peak voltage of 20-85 kV, rise time (between 10% and 90% of the peak voltage) of 2-3 ns, and pulse repetition rate of 10 Hz. The electrode assembly is enclosed within a grounded stainless steel chamber with a volume of approximately 1.7 L, designed to facilitate electrode connection to the coaxial high voltage transmission line, and reduce the electromagnetic noise produced by the discharge. The chamber is equipped with 4 opposing quartz windows providing optical access for the laser beam and for plasma emission imaging. Each of the 2 quartz windows along the beam path are located about 7.5 cm away from the beam focus, such that any weak induced electric field, combined with the low laser intensity at these optical surfaces, is anticipated to produce a negligible contribution to the signal. A 4-Picos Stanford ICCD camera is used to make line-of-sight broadband emission images of the discharge, integrated over 10 ns. The present measurements have been done in synthetic air at a flow rate of 1 slpm. The discharge voltage waveforms are measured by a custom-designed high-voltage probe (a capacitive divider integrated into the high voltage transmission line, coupled to a commercial 400 MHz bandwidth low-voltage probe). The waveforms are recorded by a LeCroy WaveRunner 640Zi oscilloscope with a 4 GHz bandwidth and 20 GS/s sampling frequency. Figure 1 also illustrates the laser beam path used for E-FISH electric field measurements.

The E-FISH optical setup, shown in Fig. 2, is similar to the one used in [23], and essentially identical to that used in our recent work [24]. The vertically polarized probe laser beam (1064 nm fundamental output of an Ekspla PL2241B laser, pulse duration 30 ps, pulse energy 1.8 mJ) is directed horizontally along the discharge vertical center plane, and is focused on the discharge centerline by a 30 cm focal distance lens (see Fig. 2). For all the experiments conducted, the electric field is probed at a distance z=3 mm from the high-voltage electrode tip with a measurement resolution – given by the confocal beam parameter [18,25] – of approximately $b \approx 2.4$ mm. A long pass filter placed after the focusing lens blocks the stray second harmonic light generated in the optical system. After the discharge chamber, the beam is collimated by a 15 cm focal distance lens, and the second harmonic signal is separated from the fundamental probe beam using a dichroic mirror and a dispersive prism, as shown in Fig. 2. The intensity of the residual 1064 nm is monitored by a photodiode (Thorlabs DET10A, rise time 1 ns). The vertically polarized 532 nm signal, proportional to the square of the vertical electric field in the discharge, is isolated by a polarizer and detected by a photomultiplier tube (PMT, Hamamatsu IR H7422-50P, rise time 1 ns). An iris and a 532 nm centered bandpass filter (FWHM 10 nm) are attached to the entrance of the PMT for further stray light rejection. The photodiode and PMT signals are monitored by the same oscilloscope used for the voltage measurements. A separate test for PMT saturation is performed for the case which produced the strongest signals (i.e. highest applied peak voltage). The measurement is performed twice, the second time adding an OD 1 neutral density filter in front of the PMT to attenuate the signal such that it falls within the linear response of the PMT.

The attenuated signal and the original signal (corrected by the attenuation factor of the filter) are verified to be in close agreement.

Due to a significant timing jitter between the HV pulse and the laser, signal waveforms are saved on every laser shot and sequenced only during the post-processing stage. Furthermore, since this jitter exists on the order of ~1 μs, the oscilloscope is pre-programmed to record only those signals in which the delay between the discharge (high-voltage probe) and the laser pulse occurs within a few tens of ns. By introducing this 'time-filter', the amount of data collected is significantly reduced. Corresponding high-voltage probe, PMT and photodiode time traces are saved for a total of between 1000 – 2500 laser shots per run, with each run lasting for a minimum of 30 min. These signals are then time-integrated, before the PMT waveforms are re-ordered based on their timing relative to the high-voltage pulse.

With this procedure, there are two limitations to the time resolution which can be achieved. First, the intrinsic discharge jitter within the voltage pulse and the laser duration introduces a physical limitation (~100 ps). This estimate is obtained by monitoring the timing stability of the discharge initiation based on plasma emission images. Second, related to the μs scale timing jitter, the number of laser shots acquired at each time instant can be very low (even zero) and yields an equivalent temporal resolution of up to 100 ps, which is lower than that based on the sampling rate of the oscilloscope (i.e. 50 ps). A time-binning approach is discussed in Section 3 to address this limitation.

As given in Eq. (1) below, the electric field is computed by taking the square root of the second harmonic signal normalized by the corresponding photodiode signal so as to account for fluctuations in the laser intensity. Absolute field information is obtained by calibration against a Laplacian field generated for a relatively low pulse peak voltage, 20 kV, when no plasma is generated in the discharge gap (as discussed further in section 3). COMSOL simulations, based on the Poisson equation are performed in order to obtain quantitative Laplacian field values for comparison with the E-FISH data. These simulations also take into account the complex geometry of the reactor and its material characteristics. To ensure better consistency with the experiments, the value of the electric field strength used for calibration is calculated by averaging the COMSOL field data over the confocal beam parameter at the measurement focal point (i.e. z=3 mm below the high voltage electrode).

3. Results and Discussion

Figure 3 shows plasma emission images, corresponding mainly to the second positive system of N_2, integrated over the entire voltage pulse duration (10 ns), and taken at different peak applied voltages. These images provide a visual description of the discharge at the early stages of its development and serve as a guide in the interpretation of the electric field data. No emission is observed for the lowest peak applied voltage of 20 kV, indicative of an electrostatic field or a very weak discharge. The existence of a discharge becomes evident as the applied voltage is gradually increased, with the spatial extent of the plasma within the gap displaying a direct dependence on the peak applied voltage.

The intensity of the vertically polarized 532 nm, E-FISH signal, $I_z^{(2\omega)}$, is given by,

$$I_z^{(2\omega)} \propto \left[\chi^{(3)}(2\omega, 0, \omega, \omega) \cdot N \cdot E_z^{ext} \cdot I_z^{(\omega)} \cdot L\right]^2 \left[sinc\left(\frac{\Delta k \cdot L}{2}\right)\right]^2 \quad (1)$$

In Eq. (1), E^{ext} represents the electric field to be measured, $I_z^{(\omega)}$ is the intensity of the vertically-polarized 1064 nm probe laser, $\chi^{(3)}$ is the third-order nonlinear susceptibility, N is the gas number density, L is the confocal beam parameter and Δk is the difference between the fundamental and second harmonic wave vectors. Here the z-axis is defined as the vertical axis, with z=0 corresponding to the tip of the high-voltage electrode.

Figure 4(a) compares the square root of the E-FISH signals at a peak voltage of 20 kV (both single-shot and 1 ns time-averaged) with the corresponding averaged Laplacian field calculated from the high-voltage probe waveform, using the COMSOL simulations described earlier. For this lowest peak voltage case, the time-averaged E-FISH signal is obtained by placing the sequenced, time-integrated PMT signals into 1 ns 'time-bins' and taking the mean value of the signals in each time-bin. Such a post-processing procedure has also been used in previous work [20,21]. While this entails a slight loss of time resolution, it is deemed necessary since it reduces the random uncertainty of the measurement by ensuring a larger number of laser shots per time-bin. For a 200 ps time-bin, there is a minimum of 1 laser shot per time-bin for the entire measurement interval; this figure rises to 10 laser shots if a 1 ns time-bin is implemented. Achieving a lower uncertainty is particularly crucial for this case, since it forms the calibration basis for the higher voltages. More importantly, a 1 ns time-bin at these conditions is appropriate, since the electric field is varying relatively slowly. It can be seen that the 1 ns time-averaged signal follows the voltage rise very closely, although a systematic deviation is observed during the voltage fall (also evident from the single shot data). This could be due to two possible reasons: an imperfect spectral response of the high voltage probe, which would imply an inability to accurately track the decay of the HV pulse, or, the presence of space charge from a weak corona discharge formation near the high-voltage electrode tip, which results in a lower electric field at the measurement location. Therefore, only the data points taken during the voltage rise (up to 90% of the peak value) are used for the Laplacian field calibration. Figure 4(b) shows that the square root of the 1 ns time-averaged E-FISH signal obeys a linear dependence with the corresponding Laplacian field values, as expected from Eq. (1). An acknowledged limitation of this calibration approach is that the measurements of high peak electric fields (typical of those during the fast ionization wave) rely on an extrapolation of the calibration curve by up to more than an order of magnitude. This is inevitable given that sustaining a Laplacian field at higher electric fields is not feasible in the present geometry, due to the plasma generation in the vicinity of the high-voltage electrode tip [4].

Figure 5 plots the absolute electric field strengths 3 mm below the pin electrode measured by the E-FISH diagnostic, along with the corresponding averaged Laplacian fields for peak applied voltages ranging from 28 kV to 85 kV. The Laplacian field values are calculated from the high-voltage probe waveforms using COMSOL simulations, as in Fig. 4. Both single-shot and smoothed E-FISH data are presented for all cases. As opposed to the 20 kV case, a combination of the rapidly changing electric field profiles associated with the higher peak voltages and limited laser shot statistics favors the interpretation of the electric field data using the single-shot (rather than bin-averaged) data in order to gain maximum temporal information. Smoothed data curves are also included but are only meant to serve as an aid for visualizing the shape of these different electric field profiles. The smoothing algorithm employed is therefore chosen with the aim of preserving the time resolution of the single shot measurements.

Several notable differences among the five data sets shown in Fig. 5, as well as the Laplacian field for the peak voltage of 20 kV, plotted in Fig. 4(a), are apparent. For a peak voltage

of 28 kV (see Fig. 5(a)), it can be seen that the peak electric field based on single shot data, approximately 140 kV/cm, exceeds the peak Laplacian field by an order of magnitude. Figure 3(c) indicates that at these conditions the plasma is generated near the high-voltage electrode, but the resulting ionization wave does not propagate far beyond the laser beam location 3 mm below the high-voltage electrode tip. Therefore, the observed electric field overshoot represents the field ahead of the ionization wave front, without the precipitous drop indicative of significant ionization and plasma self-shielding behind the wave. The fact that the electric field exceeds the applied Laplacian field during the entire duration of the voltage pulse suggests that the ionization wave is approaching the location of the laser beam relatively slowly, and does not fully traverse it. For the case of 40 kV (see Fig. 5(b)), with a nominal peak field of 160 kV/cm, the rapid electric field drop following the initial overshoot, occurring on the time scale of ~ 1 ns, becomes well-pronounced. In this case, the emission image in Fig. 3(e) reveals that at these conditions the ionization wave propagates significantly further toward the grounded electrode and traverses the laser beam, such that it is probing the regions both ahead of the wave and behind the ionization front. After the field reduction caused by the plasma self-shielding, the electric field remains below or near the Laplacian field for the remainder of the voltage pulse. In both these cases (28 kV and 40 kV), the peak measured electric field values are close to each other, approximately 130-160 kV/cm, and the electric field peaks are resolved relatively well.

As the peak applied voltage is increased further to 56 kV, the rapid electric field reduction behind the wave front becomes even more pronounced, such that the field is reduced to near detection limit (see Fig. 5(c)). This indicates a more significant plasma self-shielding caused by the charge separation behind the wave, showing that the ionization front propagates even further away from the high-voltage electrode, consistent with the plasma emission image in Fig. 3(f). The amplitude of the electric field overshoot in this case is about 200 kV/cm. Note that at these conditions, both ionization and plasma self-shielding occur so rapidly that the electric field overshoot may no longer be fully resolved in time given our estimated time resolution of 150 ps. Approximately 1.5 ns after the plasma becomes self-shielded, a well-pronounced secondary rise of the electric field is detected. Based on the plasma emission images taken at similar conditions [4], and on our previous measurements of electric field in a fast ionization wave in a long discharge tube [24], this corresponds to the moment when the ionization wave has reached the grounded electrode. This initiates intense secondary electron emission from the cathode and the propagation of a backward neutralization wave (return stroke). At this state, the electric field in the gap approaches the applied Laplacian field and the discharge becomes quasi steady-state. The different stages of the discharge development are labeled in Fig. 5(c)). These experimental data are qualitatively consistent with the discharge modeling predictions for a pulse peak voltage of 50 kV with a rise time of 2 ns, applied across a 10 mm gap in [4] and [10].

At higher peak applied voltages, 68 kV and 85 kV, the behavior of the electric field ahead and behind the ionization wave propagating across the discharge gap remains fairly similar to the 56 kV case (compare Figs. 5(c-e)). As the peak voltage is increased, the ionization wave speed also grows, such that the time interval between the plasma self-shielding behind the wave front and the arrival of the wave to the grounded electrode becomes shorter (see Figs. 5(d,e)). For the same reason, the transient electric field overshoot across the wave occurs over a shorter time scale; at 85 kV, the average speed is estimated to be 1 cm/ns. The electric field overshoot remains approximately the same, 180-210 kV/cm. In spite of the relatively limited laser shot statistics of the data sets at the highest voltages, it should be noted that the repeatability of the experiments,

and in particular the peak field values is very good. Peak field values measured from multiple experiments exhibited close agreement to within less than 10%.

At these very high voltages, two additional points must be stressed. First, the field just behind the ionization wave front increases with peak voltage reaching about 20 kV/cm at 85 kV. Very strong overvoltage appears to reduce the field shielding effect, such that the electric field penetrates into the plasma region behind the wave, contrary to classical, low overvoltage streamers [28]. Second, the growth rate of the field before the wave front crosses the laser beam 3 mm from the pin electrode is much more pronounced at higher peak voltages. Starting from about 15 kV/cm/ns at 40 kV, it reaches approximately 70 kV/cm/ns at 85 kV. This means that, before the wave front reaches 3 mm, the field is already largely enhanced and no longer purely Laplacian. The space charge located in the front is distributed in such a way that the field can be detected over longer distances.

4. Summary

In this work, the time-resolved electric field in the fast ionization wave of a diffuse ns pulse discharge plasma generated in atmospheric pressure air is measured using the ps E-FISH diagnostic over a wide range of pulse peak voltages. The electric field is measured 3 mm from the pin (high-voltage) electrode and placed on an absolute scale by Laplacian field calibration, using electrostatic field simulations. At relatively low peak voltages, when the plasma is generated only near the pin electrode, the ionization wave does not travel beyond the laser beam location. At these conditions, the electric field is measured ahead of the ionization wave during the entire voltage pulse, exhibiting a strong field enhancement compared to the Laplacian field. As the peak voltage is increased, the ionization wave propagates further toward the grounded electrode, such that the electric field is measured both ahead of the wave and behind the ionization wave front, where the field drops rapidly due to charge separation and plasma self-shielding, to near detection limit. The results indicate that the ionization wave speed, the field overshoot in the wave front, and its propagation distance are increase with the applied peak voltage. At the highest peak voltages, the field growth rate ahead of the wave front reaches about 250 kV/cm/ns and the field behind the ionization front increases up to 20 kV/cm. The results show both spreading of the space charge and a reduction of the plasma shielding effect which suggest higher electrical and chemical activity in the plasma than in classical low overvoltage streamers. When the wave reaches the grounded electrode and secondary electron emission begins, the discharge transitions into a quasi-steady-state (conduction) phase, and the electric field in the discharge gap follows the applied voltage waveform during the rest of the pulse.

The peak electric field in the wave front measured at the present conditions based on single shot data appears to be moderately affected by the applied peak voltage. However, at high peak voltages, the transient electric field overshoot in the wave front may not be fully resolved, due to insufficient laser shot acquisition, intrinsic discharge jitter (< 100 ps) and the finite sampling rate of the oscilloscope (50 ps). Temporal resolution in the range of tens of ps is critical for fully resolving the ionization wave structure in diffuse atmospheric air plasmas generated at these high over-voltages. The present approach can be used to measure different components of the electric field vector as well as the spatial distribution of the electric field. Future work also needs to include measurements of the second harmonic signal distribution along the laser beam, induced by a known Laplacian field [25], to quantify the contribution of different regions of the plasma more accurately. This work represents a significant advance in non-intrusive, quantitative characterization of highly transient, diffuse ionization wave plasmas in atmospheric pressure air.

The present data can also be used for quantitative validation of kinetic models of ns pulse breakdown in atmospheric air plasmas, which has relied primarily on qualitative comparison with the plasma emission images.

5. Acknowledgments

This work was supported by the French National Research Agency, ANR-16-CE30-0004 (ASPEN) and ANR-13-BS09-0014 (EXFIDIS) research programs, LabEx Plas@Par and the French–Russian international laboratory LIA KaPPA 'Kinetics and Physics of Pulsed Plasmas and their Afterglow'. The experiments were conducted at the Centre Laser de l'Université Paris Sud (CLUPS/LUMAT FR 2764). The authors are thankful to Dr. Cyril Drag for the use of equipment essential for conducting this study, and to Dr. Michel Broquier and Dr. Gilles Grégoire for help in setting up these experiments. The support of Prof. Adamovich by the Ecole Polytechnique Gaspard Monge Visiting Professor (GMVP) Program is gratefully acknowledged.

References

1. S.M. Starikovskaia, N.B. Anikin, S.V. Pancheshnyi, D.V. Zatsepin and A.Yu. Starikovskii, "Pulsed breakdown at high overvoltage: development, propagation and energy branching", *Plasma Sources Science and Technology* 10 (2001) 344
2. P. Tardiveau, N. Moreau, S. Bentaleb, C. Postel, and S. Pasquiers, "Diffuse mode and diffuse-to-filamentary transition in a high pressure nanosecond scale corona discharge under high voltage", *Journal of Physics D: Applied Physics* 42 (2009) 175202
3. A. N. Lagarkov, and I. M. Rutkevich, "Ionization waves in electrical breakdown of gases", Springer Science & Business Media, (2012)
4. P. Tardiveau, L. Magne, E. Marode, K. Ouaras, P. Jeanney, and B. Bournonville, "Sub-nanosecond time resolved light emission study for diffuse discharges in air under steep high voltage pulses", *Plasma Sources Science and Technology* 25 (2016) 054005
5. D.Z. Pai, G.D. Stancu, D.A. Lacoste, and C.O. Laux, "Nanosecond repetitively pulsed discharges in air at atmospheric pressure - the glow regime", *Plasma Sources Science and Technology* 18 (2009) 045030
6. D.Z. Pai, D.A. Lacoste, and C.O. Laux, "Transitions between corona, glow, and spark regimes of nanosecond repetitively pulsed discharges in air at atmospheric pressure", *Journal of Applied Physics* 107 (2010) 093303
7. D.Z. Pai, D.A. Lacoste, and C.O Laux, "Nanosecond repetitively pulsed discharges in air at atmospheric pressure - the spark regime", *Plasma Sources Science and Technology* 19 (2010) 065015
8. F. Tholin and A. Bourdon, "Simulation of the stable 'quasi-periodic' glow regime of a nanosecond repetitively pulsed discharge in air at atmospheric pressure", *Plasma Sources Science and Technology* 22 (2013) 045014
9. F. Tholin and A. Bourdon, "Simulation of the hydrodynamic expansion following a nanosecond pulsed spark discharge in air at atmospheric pressure", *Journal of Physics D: Applied Physics* 46 (2013) 365205

10. F. Pechereau, P. Le Delliou, J. Jánský, P. Tardiveau, S. Pasquiers, and A. Bourdon, "Large conical discharge structure of an air discharge at atmospheric pressure in a point-to-plane geometry", *IEEE Transactions on Plasma Science* 42 (2014) 2346
11. N. Y. Babaeva, and G. V. Naidis, "Simulation of subnanosecond streamers in atmospheric-pressure air: Effects of polarity of applied voltage pulse", *Physics of Plasmas 23*(8) (2016) 083527
12. D. V. Beloplotov, I. M. Lomaev, D. A. Sorokin and V. F. Tarasenko, "Displacement current during the formation of positive streamers in atmospheric pressure air with a highly inhomogeneous electric field", *Physics of Plasmas 25*(8) (2018) 083511.
13. S.M. Starikovskaia, "Plasma-assisted ignition and combustion: nanosecond discharges and development of kinetic mechanisms", *Journal of Physics D: Applied Physics* 47 (2014) 353001
14. A.G. Rep'ev and P.B. Repin, "Spatiotemporal Parameters of the X-ray Radiation from a Diffuse Atmospheric-Pressure Discharge", *Technical Physic*s 53 (2008) 73
15. T. Shao, C. Zhang, Z. Niu, P. Yan, V.F. Tarasenko, E.Kh. Baksht, I.D. Kostyrya, and V. Shutko, "Runaway electron preionized diffuse discharges in atmospheric pressure air with a point-to-plane gap in repetitive pulsed mode", *Journal of Applied Physics* 109 (2011) 083306
16. J.-M. Pouvesle, S. Iseni, S. Dozias, E. Robert, "Experimental Study Of An Ultra-Fast Atmospheric Pressure Air Discharge In A Pin-To-Plate Geometry", 2017 IEEE International Conference on Plasma Science (ICOPS), 21-25 May 2017, Atlantic City, NJ, USA
17. G. Gaborit, P. Jarrige, F. Lecoche, J. Dahdah, E. Duraz, C. Volat, and L. Duvillaret, "Single Shot and Vectorial Characterization of Intense Electric Field in Various Environments with Pigtailed Electrooptic Probe", *IEEE Transactions on Plasma Science* 42 (2014) 1265
18. A. Dogariu, B.M. Goldberg, S. O'Byrne, and R.B. Miles, "Species-independent femtosecond localized electric field measurement", *Physical Review Applied* 7 (2017) 024024
19. B.M. Goldberg, T.L. Chng, A. Dogariu, and R.B. Miles, "Electric field measurements in a near atmospheric pressure nanosecond pulse discharge with picosecond electric field induced second harmonic generation", *Applied Physics Letters* 112 (2018) 064102
20. M. Simeni Simeni, B. Goldberg, I. Gulko, K. Frederickson, and I.V. Adamovich, "Sub-Nanosecond Resolution Electric Field Measurements During Ns Pulse Breakdown in Ambient Air", *Journal of Physics D: Applied Physics* 51 (2018) 01LT01
21. M. Simeni Simeni, Y. Tang, K. Frederickson, and I.V. Adamovich, "Electric Field Distribution in a Surface Plasma Flow Actuator Powered by Ns Discharge Pulse Trains", *Plasma Sources Science and Technology* 27 (2018) 104001
22. B. Goldberg, S. Reuter, and A. Dogariu, "1-D Electric Field Measurements Using Field Induced Second Harmonic Generation", 60th Annual Meeting of the APS Division of Plasma Physics, November 5-9, 2018, Portland, OR, USA
23. B.M. Goldberg, T.L. Chng, A. Dogariu, and R.B. Miles, "Electric field measurements in a near atmospheric pressure nanosecond pulse discharge with picosecond electric field induced second harmonic generation", *Applied Physics Letters* 112 (2018) 064102
24. Chng, T. L., Orel, I., Starikovskaia, S. M., & Adamovich, I. V. "Electric Field Induced Second Harmonic (E-FISH) Generation for Characterization of Fast Ionization Wave Discharges at Moderate and Low Pressures", *Plasma Sources Science and Technology,* 28 (2019) 045004

25. I. J. Bigio, R. S. Finn, and J. F. Ward, “Electric-field induced harmonic generation as a probe of the focal region of a laser beam”, *Applied Optics* 14 (1975) 336

26. M. Simeni Simeni, E. Baratte, C. Zhang, K. Frederickson, and I.V. Adamovich, “Electric Field Measurements in Nanosecond Pulse Discharges in Air over Liquid Water Surface”, *Plasma Sources Science and Technology* 27 (2018) 015011

27. I.V. Adamovich, T. Li, and W.R. Lempert, “Kinetic Mechanism of Molecular Energy Transfer and Chemical Reactions in Low-Temperature Air-Fuel Plasmas”, *Philosophical Transactions of the Royal Society A* 373 (2015) 20140336

28. Y. P. Raizer, “Gas discharge physics”, (1991)

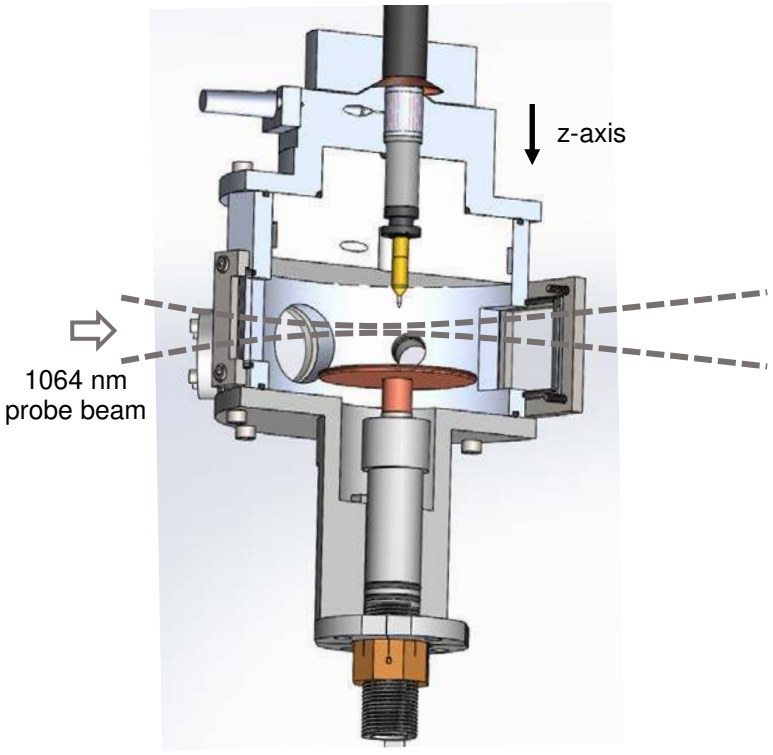

Figure 1. Schematic of the experimental apparatus [4] and the laser beam path (not to scale).

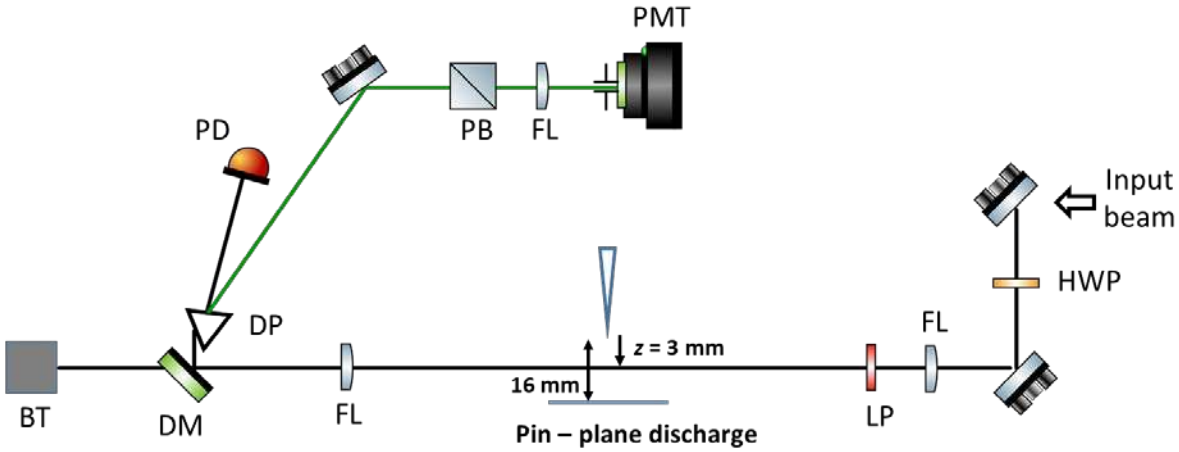

Figure 2. Schematic of ps E-FISH optical setup. Legend - BT: beam trap; DM: dichroic mirror; DP: dispersive prism; FL: plano-convex spherical lens; HWP: 1064 nm half-wave plate; LP: long pass filter; PB: 532 nm polarizer; PD: photodiode; PMT: photomultiplier tube with attached iris and 532 nm band pass filter.

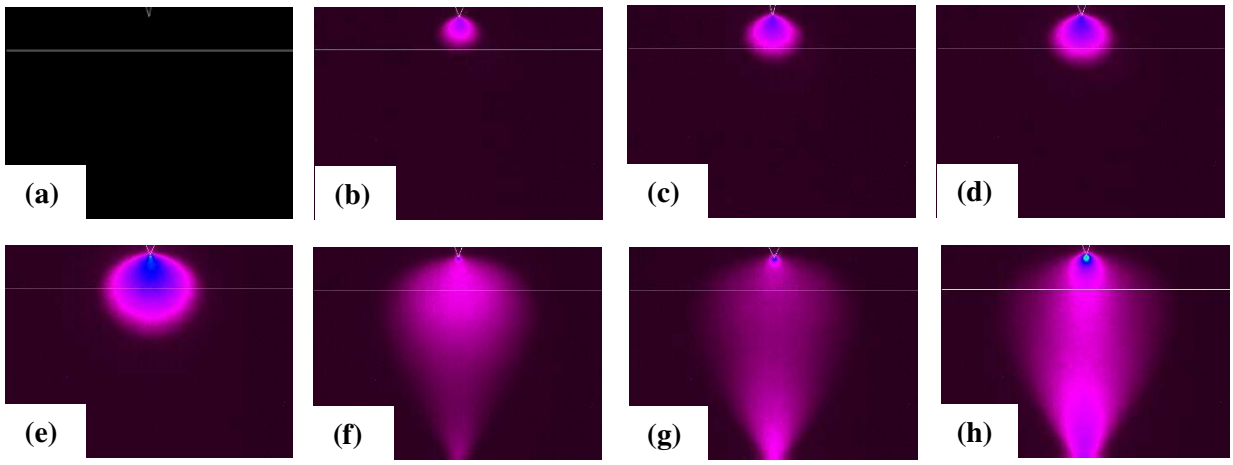

Figure 3. Emission images of the plasma for different peak applied voltages. (a): 20 kV; (b): 24 kV; (c): 28 kV; (d): 32 kV; (e): 40 kV; (f): 56 kV; (g): 68 kV; (h): 85 kV. The high-voltage electrode is outlined in white and the location of the laser beam along which the E-FISH measurements are performed (at z=3 mm) is indicated by a white line within each image. The plane electrode is located at the bottom of each image. (Images shown are to scale and correspond to a region 23 mm in width and 16.7 mm in height.)

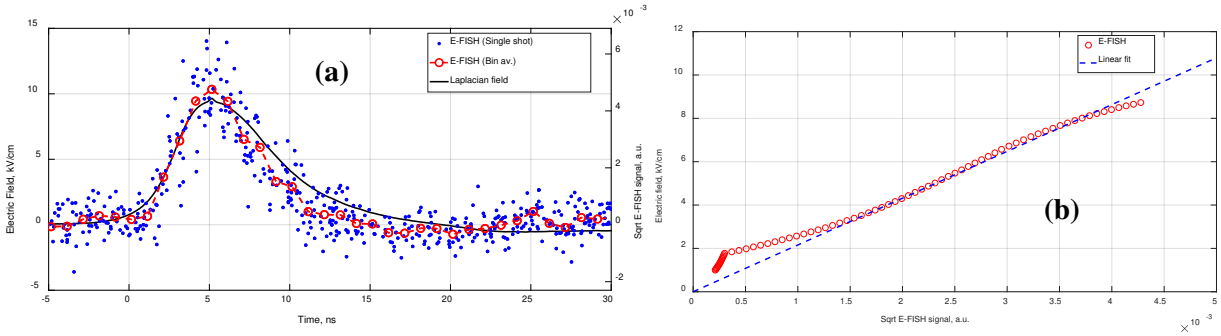

Figure 4. (a) Comparison of the square root of the E-FISH signal (single-shot and 1 ns bin average) with the Laplacian field calculated based on the applied voltage waveform and the electrode geometry. (b) Square root of the E-FISH signal vs. the Laplacian field. Peak voltage 20 kV, measurement location is 3 mm below the high-voltage electrode tip.

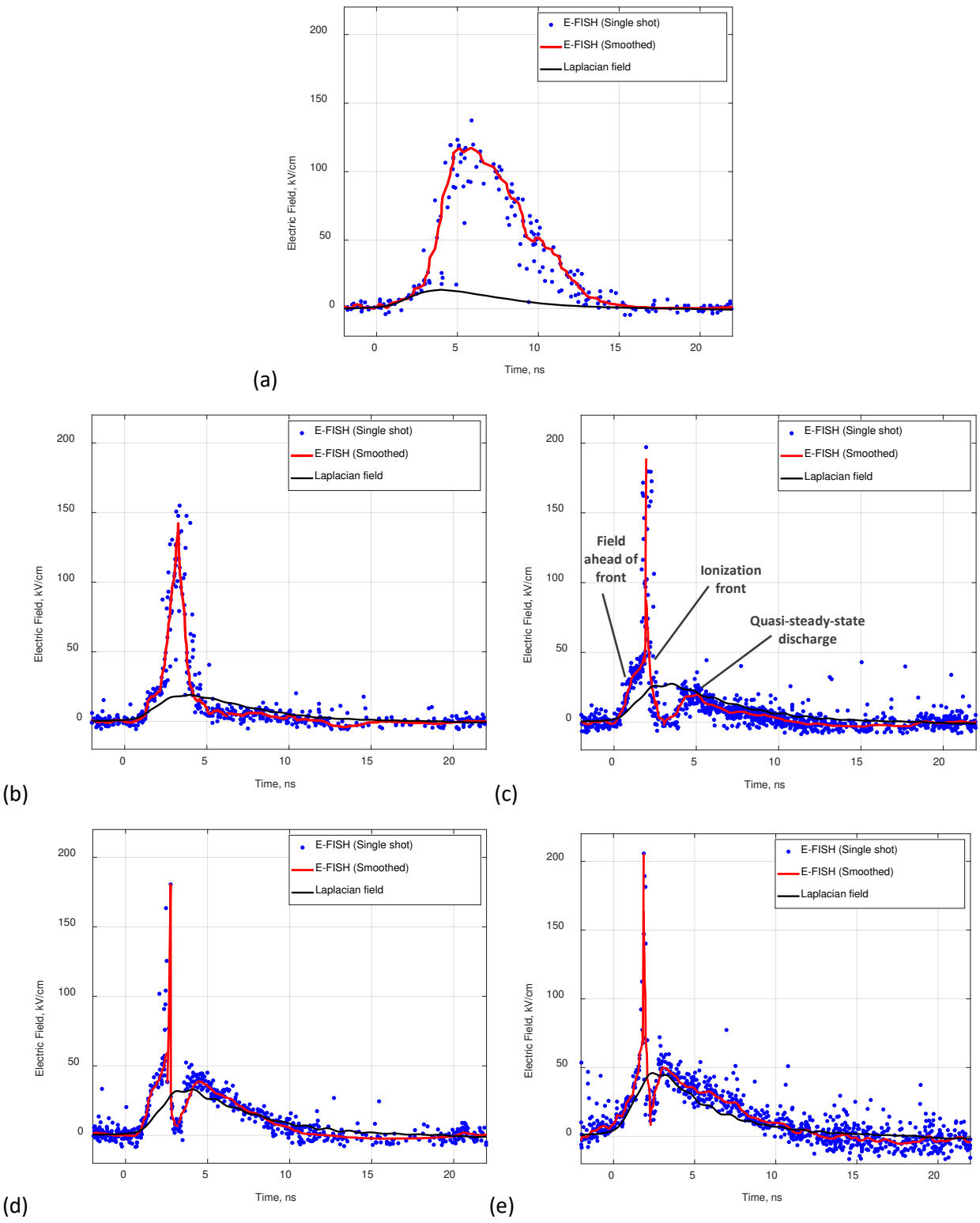

Figure 5. Single-shot and smoothed E-FISH signals plotted together with the Laplacian field based on averaged high-voltage probe waveforms. Peak voltages are (a) 28 kV, (b) 40 kV, (c) 56 kV, (d) 68 kV, and (e) 85 kV. Measurement location is 3 mm below the high-voltage electrode tip.